THE EUROPEAN
PHYSICAL JOURNAL A

Regular Article – Experimental Physics

Production of η and 3π mesons in the pd → ^{3}HeX reaction at 1360 and 1450 MeV

K. Schönning[1,a], Chr. Bargholtz[2], M. Bashkanov[3], M. Berlowski[4], D. Bogoslawsky[5], H. Calén[1], H. Clement[3], L. Demirörs[6], C. Ekström[7], K. Fransson[1], L. Gerén[2], L. Gustafsson[1], B. Höistad[1], G. Ivanov[5], M. Jacewicz[1], E. Jiganov[5], T. Johansson[1], S. Keleta[1], O. Khakimova[3], F. Kren[3], S. Kullander[1], A. Kupsc[1], A. Kuzmin[8], K. Lindberg[2], P. Marciniewski[1], B. Morosov[5], W. Oelert[9], C. Pauly[6], H. Petrén[1], Y. Petukhov[5], A. Povtorejko[5], W. Scobel[6], R. Shafigullin[10], B. Shwartz[8], T. Skorodko[3], V. Sopov[11], J. Stepaniak[4], P.-E. Tegnér[2], P. Thörngren Engblom[2], V. Tikhomirov[5], A. Turowiecki[12], G.J. Wagner[3], M. Wolke[9], J. Zabierowski[13], I. Zartova[2], and J. Złomanczuk[1]

1 Department of Physics and Astronomy, Uppsala University, Box 516, S-751 20 Uppsala, Sweden
2 Department of Physics, Stockholm University, S-106 91 Stockholm, Sweden
3 Physikalisches Institut der Universität Tübingen, D-72076 Tübingen, Germany
4 Sołtan Institute of Nuclear Studies, PL-00-681 Warsaw, Poland
5 Joint Institute for Nuclear Research, 141980 Dubna, Moscow region, Russia
6 Institut für Experimentalphysik, Universität Hamburg, D-22761 Hamburg, Germany
7 The Svedberg Laboratory, S-751 21 Uppsala, Sweden
8 Budker Institute of Nuclear Physics, 630 090 Novosibirsk, Russia
9 Institut für Kernphysik, Forschungszentrum Jülich GmbH, D-52425 Jülich, Germany
10 Moscow Engineering Physics Institute, Moscow, Russia
11 Institute of Theoretical and Experimental Physics, Moscow, Russia
12 Institute of Experimental Physics, University of Warsaw, PL-00-681 Warsaw, Poland
13 Soltan Institute of Nuclear Studies, PL-90-950 Lodz, Poland

Communicated by J. Bijnens

Abstract. The cross-sections of the $pd \to {}^3{\rm He}\,\eta$, $pd \to {}^3{\rm He}\,\pi^0\pi^0\pi^0$ and $pd \to {}^3{\rm He}\,\pi^+\pi^-\pi^0$ reactions have been measured at the beam kinetic energies $T_p = 1360$ MeV and $T_p = 1450$ MeV using the CELSIUS/WASA detector setup. At both energies, the differential cross-section $\frac{d\sigma}{d\Omega}$ of the η meson in the $pd \to {}^3{\rm He}\,\eta$ reaction shows a strong forward-backward asymmetry in the CMS. The ratio between the $pd \to {}^3{\rm He}\,\pi^+\pi^-\pi^0$ and $pd \to {}^3{\rm He}\,\pi^0\pi^0\pi^0$ cross-sections has been analysed in terms of isospin amplitudes. The reconstructed invariant-mass distributions of the $\pi\pi$, $^3{\rm He}\pi$ and $^3{\rm He}2\pi$ systems provide hints on the role of nucleon resonances in the 3π production process.

1 Introduction

The $pd \to {}^3{\rm He} + X$ reaction has long been used to study the production of charged and neutral mesons and mesonic systems. Studying reactions with ^{3}He in the final state gives insight in the reaction dynamics involving three nucleons and in meson-nucleon final-state interactions.

The $pd \to {}^3{\rm He}\eta$ reaction has been of particular interest. Several studies near the kinematic threshold [1–5], where mostly s-waves are involved in the production process, show a threshold enhancement. This enhancement has been interpreted as an indication of a quasibound $^3{\rm He}\eta$ nuclear state [6]. Measurements of the

η angular distribution at slightly higher energies from PROMICE/WASA [7] and ANKE [8] indicate the presence of p-waves at an excess energy of $Q \approx 20$ MeV, while at $Q \approx 40$ MeV even higher partial waves are required in order to describe the data. The angular distributions from refs. [7,8] have a strong forward-backward asymmetry with a backward suppression, a maximum at $\cos\theta^*_\eta \approx 0.5$ and a forward plateau or dip. At slightly overlapping excess energies, there are data from GEM [9] and Saturne [10] which disagree with the PROMICE/WASA and ANKE results. At high energies ($Q > 120$ MeV), the data bank is scarce. Backward production of η mesons in $pd \to {}^3{\rm He}\eta$ was studied at 17 different beam energies at the SPES IV spectrometer [11]. Parts of the η angular distribution at $T_p = 1450$ MeV was measured by

a e-mail: karin.schonning@fysast.uu.se

SPES III [12]. The CELSIUS/WASA Collaboration has recently studied the $pd \to {}^3$Heη reaction at two beam energies, *i.e.* $T_p = 1450$ MeV and $T_p = 1360$ MeV, which correspond to excess energies of 252 MeV and 299 MeV, respectively. The differential cross-section was measured in the backward hemisphere and at forward angles. At $T_p = 1450$ MeV, the backward points overlap with those from ref. [12]. The angular distribution at $T_p = 1360$ MeV obtained with CELSIUS/WASA is the first measured at this energy.

The direct production of three pions, *i.e.* pions which do not originate from, *e.g.*, ω or η decay, has so far received little theoretical and experimental attention. In the isobar model discussed in ref. [13], three-pion production should proceed *via* an excitation of one or two baryon resonances, like $\Delta(1232)$ or the Roper $N^*(1440)$, followed by their subsequent decays. Three-pion production in proton-proton collisions was studied at high energies [14–16] and at lower energies by CELSIUS/WASA [17]. In the latter work, the ratio between $\sigma(pp \to pp\,\pi^+\pi^-\pi^0)$ and $\sigma(pp \to pp\,\pi^0\pi^0\pi^0)$ was measured and discussed in terms of isospin amplitudes. The ratio was measured to be $6.3 \pm 0.6 \pm 1.0$ which suggests that the $N^*(1440) \to \Delta\pi$ being the leading part of the reaction mechanism, in line with the isobar model presented in ref. [13].

In the $pd \to {}^3$He$\pi\pi\pi$ case, it is straightforward to show that the total cross-sections expressed in isospin amplitudes $M_{T_{3\pi}}$ are

$$\sigma(pd \to {}^3\mathrm{He}\,\pi^+\pi^-\pi^0)$$
$$\propto \frac{2}{15}|M_1|^2 + \frac{1}{6}|M_0|^2 + \text{cross terms}, \qquad (1)$$

$$\sigma(pd \to {}^3\mathrm{He}\,\pi^0\pi^0\pi^0) \propto \frac{1}{30}|M_1|^2, \qquad (2)$$

where $T_{3\pi}$ denotes the isospin of the three pions. In the simple statistical approach as outlined by Fermi [18], all amplitudes in eq. (1) and eq. (2) are put equal and the cross terms are neglected. Though not justified, this simplification enables a rough comparison between two channels for which no other, more realistic, model exists. The cross-section ratio then becomes

$$\frac{\sigma(pd \to {}^3\mathrm{He}\,\pi^+\pi^-\pi^0)}{\sigma(pd \to {}^3\mathrm{He}\,\pi^0\pi^0\pi^0)} = 9. \qquad (3)$$

If M_0 is put to 0, the ratio becomes 4. In this work, the ratio has been estimated experimentally at 1360 MeV, which corresponds to an excess energy of $Q = 395$ MeV for $3\pi^0$ and $Q = 386$ MeV for $\pi^+\pi^-\pi^0$, and at 1450 MeV, which corresponds to $Q = 441$ MeV for $3\pi^0$ and $Q = 432$ MeV for $\pi^+\pi^-\pi^0$.

Multipion production is also interesting since it constitutes the most important background to other meson production reactions like $pd \to {}^3$Heη, $pd \to {}^3$Heω, $pd \to {}^3$HeΦ and $pd \to {}^3$He$\eta\pi^0$.

This paper is organised as follows: in the next section, the reader is introduced to the CELSIUS/WASA experiment. In sect. 3, the measurement of the $pd \to {}^3$Heη reaction is presented and in sect. 4, the $pd \to {}^3$He$\pi^0\pi^0\pi^0$

and $pd \to {}^3$He$\pi^+\pi^-\pi^0$ reactions are studied and compared. Finally the results are summarised and discussed in sect. 5.

2 The CELSIUS/WASA experiment

The measurements were carried out at the The Svedberg Laboratory in Uppsala, Sweden. The WASA detector [19] was, until June 2005, an integrated part of the CELSIUS storage ring. In the measurements presented here, a target of deuterium pellets [20,21] was used, designed for a 4π detector geometry and high luminosity.

The ^{3}He ions were detected in the Forward Detector (FD) [22], covering polar angles from $3°$ to $18°$. The FD consists of the Window Counter (FWC) for triggering, the Proportional Chamber for precise angular information (FPC), the Trigger Hodoscope (FTH) for triggering and offline particle identification and the Range Hodoscope (FRH) for energy measurements, particle identification and triggering. Mesons and their decay products are mainly detected in the central detector (CD), which consists of the Plastic Scintillating Barrel (PSB), the Mini Drift Chamber (MDC) and the Scintillating Electromagnetic Calorimeter (SEC). Charged particles, mainly pions, are discriminated from neutral ones by their signals in the PSB, that also provides azimuthal angular information and covers a polar angular range from $24°$ to $159°$. The momenta of charged particles are extracted by tracking in a magnetic field in the MDC. The SEC measures angles and energies of photons from meson decays and covers polar angles from $20°$ to $169°$.

A special trigger was developed to select events with ^{3}He in the final state, based on the condition that ^{3}He events give high-energy deposit in the FWC and that hits detected by the FWC and the consecutive detectors FTH and FRH should match in the azimuthal angle. It was carefully checked in the offline analysis that the energy deposit thresholds were set sufficiently low to accept ^{3}He ions in the full energy range, *i.e.* giving an unbiased ^{3}He sample.

In the offline analysis, the ^{3}He ions are identified in the FD by first obtaining a preliminary particle identity (PID) using the ΔE-E method. In short, we compare the light output in the detector layer where the particle stops to the light output in the preceding layer. The χ^2 of the PID hypothesis was then calculated by comparing the measured energy deposits in all detector layers traversed by the particle to the calculated energy deposits. Particle hypotheses giving a χ^2 larger than a certain maximum value were rejected. For details, see refs. [23,24].

3 The $pd \to {}^3$He η reaction

The WASA data collected at $T_p = 1360$ MeV and $T_p = 1450$ MeV correspond to excess energies $Q = 252$ MeV and $Q = 299$ MeV and to η CM momenta of $p_\eta^* = 516$ MeV/c and $p_\eta^* = 568$ MeV/c. Here and in the following, the star indicates that a kinematic variable is in the CM system.

Table 1. The constraints applied for the selection of $pd \to {}^3\text{He}\eta$, $\eta \to \gamma\gamma$. The angle $\theta_{(\gamma\gamma)mm({}^3\text{He})} < 20°$ refers to the difference between the direction of the $\gamma\gamma$ system and the missing momentum of the ${}^3\text{He}$.

${}^3\text{He}$ giving signal in the FPC and stopping in the FRH
$\geqslant 2$ photons in the SEC with $E_\gamma > 20\,\text{MeV}$;
one $\gamma\gamma$-combination fulfilling $|IM(\gamma\gamma) - m_\eta| < 150\,\text{MeV}/c^2$;
$MM^2({}^3\text{He}\gamma\gamma) < 10000\ (\text{MeV}/c^2)^2$;
$\theta_{(\gamma\gamma)mm({}^3\text{He})} < 20°$;
no overlapping hits in the PSB and the SEC;
$160° < |\phi_{lab}({}^3\text{He}) - \phi_{lab}(\gamma\gamma)| < 200°$

The WASA Forward Detector does not cover the entire ${}^3\text{He}$ phase space in the $pd \to {}^3\text{He}\eta$ reaction at these energies. The maximum emission angle of the ${}^3\text{He}$ in the laboratory system is $18.5°$ at $T_p = 1360\,\text{MeV}$ and $19.6°$ at $T_p = 1450\,\text{MeV}$ and the FD only covers angles up to $18.0°$.

In fig. 1, the acceptances at both energies are shown as a function of $\cos\theta_\eta^*$, when constraints optimised for $\eta \to \gamma\gamma$ selection (see sect. 3.1.1) are applied. The acceptance drops at high and low angles due to ${}^3\text{He}$ ions emitted at small laboratory angles, $\theta_{{}^3\text{He}} < 3°$. The middle hole in the acceptance is caused by ${}^3\text{He}$ ions emitted at large angles $\theta_{{}^3\text{He}} > 18°$. The acceptance drops at $\cos\theta_\eta^* \approx -0.75$ ($1360\,\text{MeV}$) and $\cos\theta_\eta^* \approx -0.55$ ($1450\,\text{MeV}$) are caused by ${}^3\text{He}$ ions stopping between two layers of the FRH.

3.1 Event selection

The three main decay channels of the η, *i.e.* $\eta \to \gamma\gamma$ (BR $= 39.3\%$), $\eta \to \pi^0\pi^0\pi^0$ (BR $= 32.6\%$) and $\eta \to \pi^0\pi^+\pi^-$ (BR $= 22.7\%$) have all been separated and studied with the WASA setup. In this work, we focus on $\eta \to \gamma\gamma$ since it provides a clean sample with good statistics. The simultaneous study of $\eta \to \pi^0\pi^0\pi^0$ and $\eta \to \pi^+\pi^-\pi^0$ allow valuable cross checks of the results.

### 3.1.1 $pd \to {}^3\text{He}\eta$, $\eta \to \gamma\gamma$

In this case all final-state particles —one ${}^3\text{He}$ and two photons— can be measured with good acceptance. We thus have an over-constrained measurement and thereby, we can check if an event is consistent with the expected kinematics. This reduces the background significantly and gives a clean sample.

The criteria for $\eta \to \gamma\gamma$ selection are given in table 1. Assuming phase space production, they give an acceptance of 20% at $1360\,\text{MeV}$ and 14% at $1450\,\text{MeV}$.

Figure 1 shows how the acceptance varies as a function of $\cos\theta_\eta^*$. The acceptance is limited by the geometrical coverage of the FD, by photons missing the CsI modules in the calorimeter and by the efficiency reduction due to ${}^3\text{He}$ ions undergoing nuclear interaction before depositing all their energy.
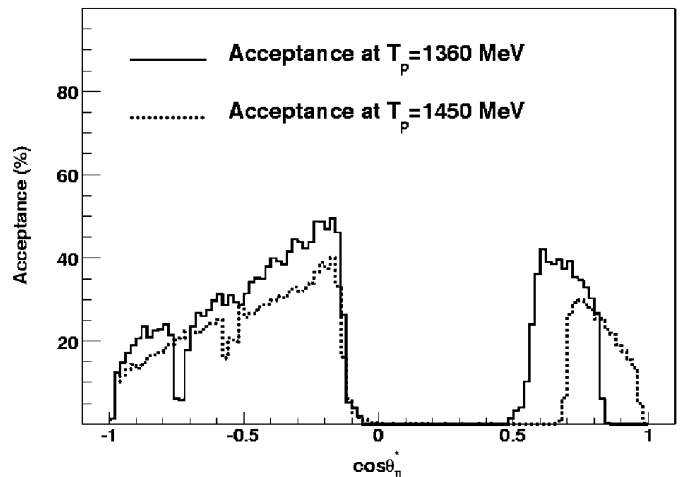
Fig. 1. The acceptance of the $pd \to {}^3\text{He}\eta$, $\eta \to \gamma\gamma$ reaction as a function of $\cos\theta_\eta^*$ at $T_p = 1450\,\text{MeV}$ (dashed line) and at $T_p = 1360\,\text{MeV}$ (solid line).
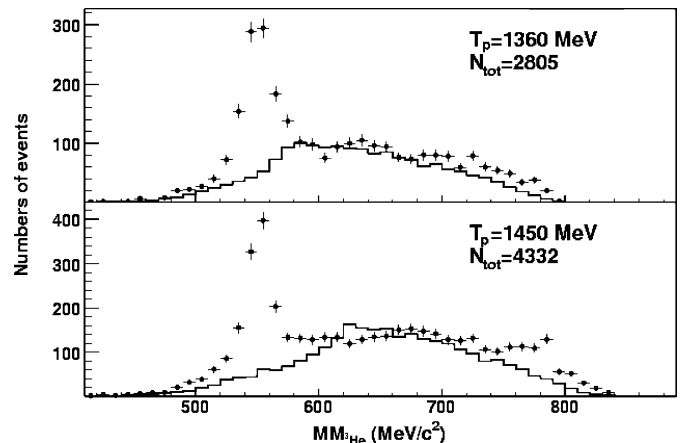
Fig. 2. The upper panel shows the WASA data sample fulfilling the constraints optimised for the selection of $\eta \to \gamma\gamma$ at $1360\,\text{MeV}$ and the lower panel shows the $1450\,\text{MeV}$ case. The solid line histograms show Monte-Carlo-simulated $pd \to {}^3\text{He}\,\pi^0\pi^0$ data fulfilling the given constraints. The spectra are not corrected for acceptance and the background simulations are scaled to fit the data.

The upper panel of fig. 2 shows the ${}^3\text{He}$ missing mass for all events fulfilling the constraints optimised for $\eta \to \gamma\gamma$ selection at $T_p = 1360\,\text{MeV}$. The bottom panel shows the $T_p = 1450\,\text{MeV}$ case. Phase space Monte Carlo simulations of the main background channel, $pd \to {}^3\text{He}\,\pi^0\pi^0$, are also shown, normalised to fit the data. They reproduce the background in the experimental data fairly well, except for an enhancement at high ${}^3\text{He}$ missing mass at $T_p = 1450\,\text{MeV}$ which is caused by $pd \to {}^3\text{He}\,\omega$, $\omega \to \pi^0\gamma$ events that accidentally satisfy the criteria. Assuming phase space $2\pi^0$ production give an acceptance of 3.6% at $T_p = 1360\,\text{MeV}$ and 4.0% at $T_p = 1450\,\text{MeV}$. Other reactions, *e.g.* $pd \to {}^3\text{He}\,\pi^0\pi^0\pi^0$, were found to give a negligible contribution to the $\eta \to \gamma\gamma$ background.

Table 2. The constraints applied for the selection of $pd \rightarrow$ $^3\mathrm{He}\eta$, $\eta \rightarrow \pi^0\pi^0\pi^0$.

^{3}He giving signal in the FPC and stopping in the FRH
$\geqslant 6$ photons in the SEC with $E_\gamma > 20\,\mathrm{MeV}$;
one $\gamma\gamma$-combination fulfilling $|IM(\gamma\gamma) - m_{\pi^0}| < 50\,\mathrm{MeV}/c^2$;
two other $\gamma\gamma$-combinations fulfilling $|IM(\gamma\gamma) - m_{\pi^0}| < 60\,\mathrm{MeV}/c^2$;
$MM^2(^3\mathrm{He}6\gamma) < 20000\,(\mathrm{MeV}/c^2)^2$;
no overlapping hits in the PSB and the SEC
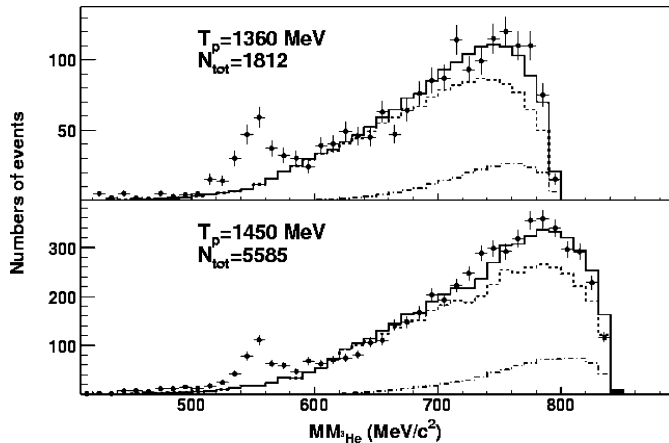
Fig. 3. The upper panel shows the data fulfilling the constraints optimised for selection of $\eta \rightarrow \pi^0\pi^0\pi^0$ at 1360 MeV and the lower panel shows the 1450 MeV case. The dotted line histograms show Monte-Carlo-simulated $pd \rightarrow {}^3\mathrm{He}\,\pi^0\pi^0\pi^0$ data fulfilling the given constraints, the dash-dotted histogram simulated $pd \rightarrow {}^3\mathrm{He}\pi^0\pi^0\pi^0\pi^0$ data and the solid line the sum of $3\pi^0$ and $4\pi^0$ production. The spectra are not corrected for acceptance and the background simulations are scaled to fit the data.

3.1.2 $pd \rightarrow {}^3\mathrm{He}\eta$, $\eta \rightarrow \pi^0\pi^0\pi^0$

In this case we need six photons from the three π^0 decays in order to indentify the events. The Scintillator Electromagnetic Calorimeter (SEC) has a small "hole" in the backward part and one large in the forward part, where the photons escape undetected. Therefore, in most $\eta \rightarrow \pi^0\pi^0\pi^0$ events at least one, but often several, photons escape detection. The acceptance is therefore significantly reduced compared to the $\eta \rightarrow \gamma\gamma$ case.

The constraints optimised for $\eta \rightarrow \pi^0\pi^0\pi^0$ selection are given in table 2.

Assuming phase space production, this gives a total acceptance of 5.7% at $T_p = 1360\,\mathrm{MeV}$ and 3.6% $T_p = 1450\,\mathrm{MeV}$. The main background channel is direct $pd \rightarrow {}^3\mathrm{He}\,\pi^0\pi^0\pi^0$ production. At high missing masses, there is also a contribution from $pd \rightarrow {}^3\mathrm{He}\,\pi^0\pi^0\pi^0\pi^0$ production, which will be discussed in sect. 4.1. The acceptance for direct $3\pi^0$ production at $T_p = 1360\,\mathrm{MeV}$ is 11.7% and 10.3% at $T_p = 1450\,\mathrm{MeV}$, if phase space production is assumed.
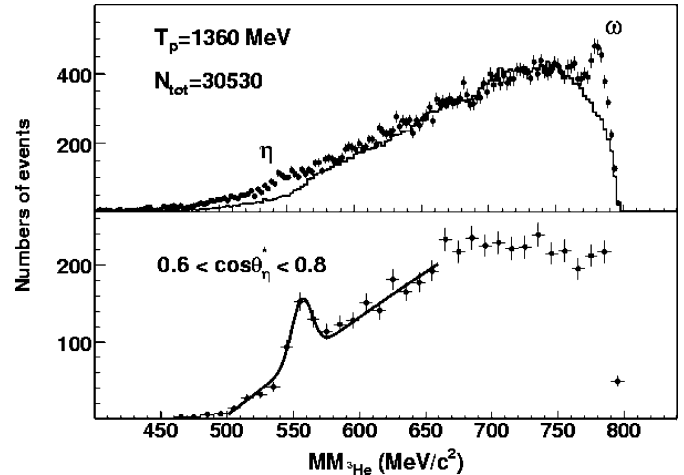
The upper panel of fig. 3 shows the ^{3}He missing mass for all events fulfilling the constraints optimised for

Table 3. The constraints applied for the selection of $pd \rightarrow$ $^3\mathrm{He}\eta$, $\eta \rightarrow \pi^+\pi^-\pi^0$.

^{3}He giving signal in the FPC and stopping in the FRH
$\geqslant 2$ photons in the SEC with $E_\gamma > 20\,\mathrm{MeV}$;
one $\gamma\gamma$-combination fulfilling $|IM(\gamma\gamma) - m_{\pi^0}| < 45\,\mathrm{MeV}/c^2$;
$MM(^3\mathrm{He}\pi^0) > 250\,\mathrm{MeV}/c^2$;
$\geqslant 2$ hits in the PSB;
$E_{tot}(\mathrm{SEC}) < 900\,\mathrm{MeV}$

Fig. 4. The upper panel shows all data at $T_p = 1360\,\mathrm{MeV}$ that satisfy the criteria optimised for $pd \rightarrow {}^3\mathrm{He}\,\eta$, $\eta \rightarrow \pi^+\pi^-\pi^0$ selection. The solid line represents Monte Carlo simulations of direct $\pi^+\pi^-\pi^0$ production. These spectra are not corrected for acceptance and the background simulations are scaled to fit the data. The lower panel shows the same thing but in the angular region $0.6 < \cos\theta_\eta^* < 0.8$. The line is the result of a fit of a Gaussian peak on top of a polynomial background.

$\eta \rightarrow \pi^0\pi^0\pi^0$ at $T_p = 1360\,\mathrm{MeV}$ and the bottom panel shows the same but for $T_p = 1450\,\mathrm{MeV}$.

3.1.3 $pd \rightarrow {}^3\mathrm{He}\eta$, $\eta \rightarrow \pi^+\pi^-\pi^0$

The criteria optimised for $\eta \rightarrow \pi^+\pi^-\pi^0$ are given in table 3. The last one, requiring the total energy deposit in the SEC to be smaller than 900 MeV, rejects time-overlapping events, *i.e.* chance coincidences. The selection criteria give altogether an acceptance of 18% at $T_p = 1360\,\mathrm{MeV}$ and 12% at $T_p = 1450\,\mathrm{MeV}$.

The main background comes from non-resonant $\pi^+\pi^-\pi^0$ production. The acceptance for the $pd \rightarrow {}^3\mathrm{He}\,\pi^+\pi^-\pi^0$ reaction when the given constraints are applied and phase space production is assumed, is 35% at $T_p = 1360\,\mathrm{MeV}$ and 31% at $T_p = 1450\,\mathrm{MeV}$.

The upper panel of fig. 4 shows all data at $T_p = 1360\,\mathrm{MeV}$ that fulfill the cuts optimised for $pd \rightarrow {}^3\mathrm{He}\,\eta$, $\eta \rightarrow \pi^0\pi^+\pi^-$ selection. It is difficult to separate the η events from the background, partly due to the small signal-to-background ratio and partly due to the broad η peak. However, in individual regions in $\cos\theta_\eta^*$, the η events

appear in a peak and can be separated from the background with reasonable accuracy. An example is shown in the lower panel of fig. 4. The η peak for the full $\cos\theta_\eta^*$ range, shown in the upper panel of fig. 4, is broader than the η peak in an individual $\cos\theta_\eta^*$ interval, shown in lower panel of fig. 4. The broadness of the peak in the full $\cos\theta_\eta^*$ range is due to a small dependence of the η peak position on $\cos\theta_\eta^*$. This in turn is an effect of the calibration constants, which are slightly dependent on energy. This was also observed in ref. [7], but there the effect was much stronger. Here it is negligible for small lab angles $\theta_{{}^3\text{He}}^{lab}$ where the variation in $T_{{}^3\text{He}}$ is small. For large $\theta_{{}^3\text{He}}^{lab}$, it gives a contribution to the systematic uncertainty of $< 3\%$.

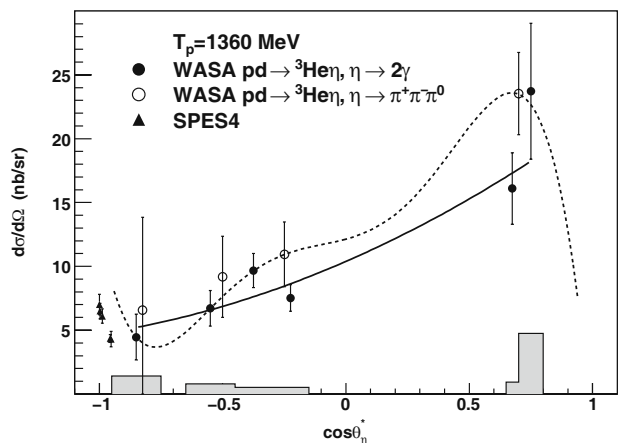## 3.2 The η angular distribution

The angular distributions were obtained by dividing the $\eta \rightarrow \gamma\gamma$ data sample into intervals of $\cos\theta_\eta^*$ where the acceptance is smooth and non-zero. The η mesons are identified by the missing-mass method in individual bins of $\cos\theta_\eta^*$, some examples are shown in fig. 5. The number of η candidates is extracted by fitting Gaussian peak on top of a polynomial background (it has been checked that in individual $\cos\theta_\eta^*$ region the background has no discontinuities). This number was then corrected for acceptance. The systematic uncertainty was estimated by fitting simulated Monte Carlo data of the main background channel (in this case $pd \rightarrow {}^3\text{He}\pi^0\pi^0$) and compare the number of η events obtained in this way to the number of η's obtained from fitting the background to a polynomial. The same procedure was repeated for the $\eta \rightarrow 3\pi$ channels. The η mesons are easier to identify in the intervals than in the cumulative spectrum (compare the upper and the lower panel of fig. 4). It turns out that the agreement in individual $\cos\theta_\eta^*$ regions is good between the $\eta \rightarrow 2\gamma$ and the $\eta \rightarrow 3\pi$ channels. This gives confidence that the cut efficiencies are well understood and that our systematic uncertainties are under control.

The normalisation was achieved by comparing data on backward going η mesons from $pd \rightarrow {}^3\text{He}\eta$ from SPES IV [11] and SPES III [12] with the corresponding data from this work using the method described in refs. [23] and [25]. The normalisation uncertainty of the measured cross-sections and is 29% at 1360 MeV and 12% at 1450 MeV.

The resulting angular distributions are shown in fig. 6 and fig. 7. The systematic uncertainties are shown as a shaded histogram in each figure. They mainly arise from the ambiguity in the background subtraction, but there is also a small contribution from the energy dependence of the calibration constants (see sect. 3.1.3). The distributions at both energies are highly anisotropic with a sharp forward-backward asymmetry. This is in line with earlier experiments, *e.g.* refs. [7–10,12], where evidence were found for several higher partial waves away from the threshold region. From comparing SPES III data with data from this work at $T_p = 1450\,\text{MeV}$, which is done in fig. 7, the conclusion is that either the two data sets
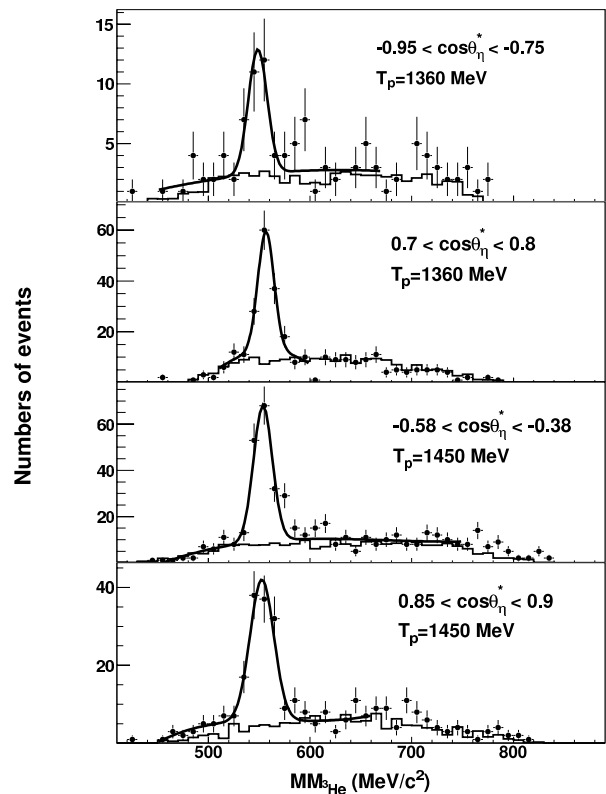
Fig. 5. The ${}^3\text{He}$ missing-mass distribution for events satisfying the constraints optimised for $\eta \rightarrow \gamma\gamma$ selection (see text) in given intervals of $\cos\theta_\eta^*$. These MM-spectra are not acceptance corrected and the background simulations are scaled to fit the data.

Fig. 6. Angular distribution of the η meson in the CM system at $T_p = 1360\,\text{MeV}$. The black dots are WASA data from the $pd \rightarrow {}^3\text{He}\eta$, $\eta \rightarrow \gamma\gamma$ channel. The error bars represent the statistical uncertainties and the grey histogram the systematical ones. The open dots are obtained with WASA data from $pd \rightarrow {}^3\text{He}\eta$, $\eta \rightarrow \pi^0\pi^+\pi^-$. The black triangles are calculated by interpolating SPES IV [11] data at $T_p = 1250\,\text{MeV}$ and $T_p = 1350\,\text{MeV}$ and SPES III data at $T_p = 1450\,\text{MeV}$. The Legendre fit represented by the solid line has been used to calculate the cross-section quoted here and the fit shown as a dashed line has been used to estimate the systematical uncertainty.
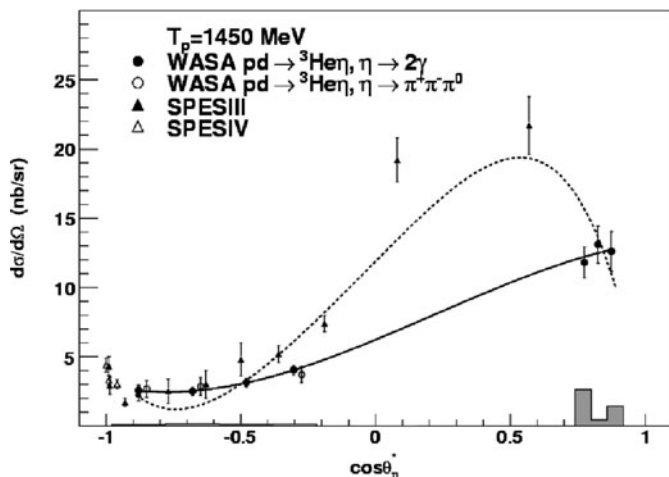
Fig. 7. Angular distribution of the η meson in the CM system at $T_p = 1450\,\mathrm{MeV}$. The black dots are WASA data from $pd \to {}^3\mathrm{He}\eta$, $\eta \to \gamma\gamma$ at $T_p = 1450\,\mathrm{MeV}$. The error bars represent the statistical uncertainties and the grey histogram the systematical. The open dots are obtained with WASA data from $pd \to {}^3\mathrm{He}\eta$, $\eta \to \pi^0\pi^+\pi^-$. The black triangles are data from SPES III [12] while the open triangles come from SPES IV [11]. The curves are results of fits of Legendre series to the WASA data (solid) and WASA plus SPES III (dashed).

are inconsistent, or there is a forward dip that is much stronger than the dip observed in refs. [7,8].

The angular distributions were fitted by a series of Legendre polynomials

$$\frac{\mathrm{d}\sigma}{\mathrm{d}\Omega}(\cos\theta_\eta^*) = \sum_{k=0}^{k_{max}} a_k P_k(\cos\theta_\eta^*) \qquad (4)$$

to the $\eta \to \gamma\gamma$ data points from WASA. The zeroth coefficient of the Legendre polynomial gives, when multiplied with 4π, the total cross-section. At 1360 MeV one obtains $\sigma_{tot} = 151.6 \pm 9.3 \pm 35.3\,\mathrm{nb}$. In addition, there is an uncertainty from the normalisation of 29%. At 1450 MeV the total cross-section is estimated to be $\sigma_{tot} = 80.9 \pm 3.6 \pm 43.0\,\mathrm{nb}$. The normalisation uncertainty is 12% at 1450 MeV.

4 Multipion production

In this section, we first study the $pd \to {}^3\mathrm{He}\,\pi^0\pi^0\pi^0$ reaction, then the $pd \to {}^3\mathrm{He}\,\pi^+\pi^-\pi^0$ reaction and finally, the two three-pion reactions are compared.

4.1 The pd $\to$ ^{3}He $\pi^0\pi^0\pi^0$ reaction

The same selection criteria are used as for the $pd \to {}^3\mathrm{He}\,\eta$, $\eta \to \pi^0\pi^0\pi^0$ case, given in table 2 of sect. 3.1.2. For the $pd \to {}^3\mathrm{He}\,\pi^0\pi^0\pi^0$ reaction, they give acceptances of 11.7% at 1360 MeV and 10.3% at 1450 MeV. There may be a large uncertainty in the acceptance of a reaction where six photons are measured. To estimate this uncertainty,

we assume that the difference in the extracted number of η mesons from $\eta \to \gamma\gamma$ and $\eta \to \pi^0\pi^0\pi^0$ is entirely caused by the ambiguities in the acceptance and that the uncertainty is the same at both energies. The uncertainty in the acceptance is then estimated to a maximum value of 20%.

The ^{3}He missing-mass distributions at both energies for all events fulfilling the constraints are shown in fig. 3 in sect. 3.1.2. The dotted line shows simulated $pd \to {}^3\mathrm{He}\,\pi^0\pi^0\pi^0$ data assuming phase space production. Simulated $3\pi^0$ data match the experimental data for low and medium missing masses (except at the η peak, which is expected), but at high MM(^{3}He), the matching between data and phase space Monte Carlo is poor.

It is reasonable to assume a contribution from $pd \to {}^3\mathrm{He}\,\pi^0\pi^0\pi^0\pi^0$, either from direct production or from production via $\eta\pi^0$ in $pd \to {}^3\mathrm{He}\,\eta\pi^0$, $\eta \to \pi^0\pi^0\pi^0$. In both reactions, eight photons are produced and the acceptance for the selection criteria in table 2 is 28% at 1360 MeV and 24% at 1450 MeV. At the highest energy, the maximum ^{3}He emission angle in the lab system is 15° in the $\eta\pi^0$ case and 18° in the $4\pi^0$ case, which means that in both cases, the WASA Forward Detector covers almost the full ^{3}He phase space. The acceptance is then nearly independent of the production mechanism.

The $4\pi^0$ distributions obtained from Monte Carlo simulations are shown as the dash-dotted line histograms in the upper and lower panel of fig. 3. Adding the contributions from $3\pi^0$ and $4\pi^0$ together gives the solid line histograms in fig. 3. We obtain $N_{4\pi^0} = 250$ at $T_p = 1360\,\mathrm{MeV}$ and $N_{4\pi^0} = 800$ at $T_p = 1450\,\mathrm{MeV}$.

The cross-section of the $pd \to {}^3\mathrm{He}\,\eta\pi^0$ reaction at $T_p = 1450\,\mathrm{MeV}$ has been measured to $\sigma_{tot} = 23.6 \pm 1.6 \pm 2.2\,\mathrm{nb}$ $\pm14\%$ by studying the $\eta \to \gamma\gamma$ decay [26].

From the known cross-section of $pd \to {}^3\mathrm{He}\,\eta\pi^0$ reaction at $T_p = 1450\,\mathrm{MeV}$ (see ref. [26]) and from the acceptance and the branching ratio of $\eta \to \pi^0\pi^0\pi^0$, the expected number of $pd \to {}^3\mathrm{He}\,\eta\pi^0$, $\eta \to \pi^0\pi^0\pi^0$ events is calculated to 700 ± 80. This explains almost fully the $N_{4\pi^0} = 800$ and it is clear that the cross-section of direct $4\pi^0$ production must be very small at 1450 MeV.

Subtracting the fitted $4\pi^0$ and $\eta\pi^0$ distributions from the experimental data gives $N_{3\pi^0} = 1400$ and $N_{3\pi^0} = 4500$ at $T_p = 1360\,\mathrm{MeV}$ and $T_p = 1450\,\mathrm{MeV}$, respectively. This corresponds to $3\pi^0$ cross-sections of 180 nb and 115 nb. The statistical uncertainty of $N_{3\pi^0}$ is given by the square root of the total number of events before the subtraction and is equal to 3% (2%) at $T_p = 1360\,\mathrm{MeV}$ ($T_p = 1450\,\mathrm{MeV}$).

It is also possible that part of the deviation from the $3\pi^0$ phase space curve in fig. 3 is due to a production mechanism that differs from phase space production. This will be discussed later in this paper. However, at least at $T_p = 1450\,\mathrm{MeV}$, the expected contribution from $pd \to {}^3\mathrm{He}\,\eta\pi^0$, $\eta \to 3\pi^0$ explain the data well and the remaining excess of events at high ^{3}He missing masses gives a small contribution to the systematic uncertainty.

At $T_p = 1360\,\mathrm{MeV}$, it is difficult to say with certainty that the excess of events at high $MM(^3\mathrm{He})$ in the upper

panel of fig. 3 are not directly produced $3\pi^0$ events. The cross-section of the $pd \rightarrow {}^3\text{He}\,\eta\pi^0$ reaction is not known, and it is therefore unclear whether a significant contribution from this reaction is to be expected. However, the mixture of $3\pi^0$ and $4\pi^0$ events reproduces the experimental distributions also at $T_p = 1360\,\text{MeV}$ very well and it is therefore reasonable to assume a contribution from $4\pi^0$ production, either from direct production or from the subsequent η decay in $\eta\pi^0$ production. We therefore take the $3\pi^0$ cross-section of 180 nb, calculated when assuming that the deviation from the $3\pi^0$ curve at large $MM({}^3\text{He})$ in fig. 3 comes from $4\pi^0$ production, as the most reliable one. The excess of events is treated as a systematic uncertainty. By assuming that all events in the upper panel of fig. 3 that do not come from $pd \rightarrow {}^3\text{He}\,\eta$, $\eta \rightarrow 3\pi^0$ are directly produced $3\pi^0$ events, $N_{3\pi^0}$ becomes 1650 which corresponds to a cross-section of 212 nb. The systematic uncertainty is then taken as the difference between the cross-sections calculated in two different ways, *i.e.* 32 nb. We assume that the uncertainty is symmetric. This is a conservative method of estimating the systematic uncertainty and other systematic contributions, *e.g* the variation in the acceptance due to reaction mechanism, should be well within the error bars estimated in this way.

We can also give a rough upper limit of the $pd \rightarrow {}^3\text{He}\,\eta\pi^0$ at 1360 MeV, which will be useful in the next section. Assuming that all the $N_{4\pi^0} = 250$ events come from $\eta\pi^0$ production, the $\sigma(pd \rightarrow {}^3\text{He}\,\eta\pi^0)$ would be 42 nb.

The total cross-section of $3\pi^0$ production then becomes $\sigma_{3\pi^0} = 180 \pm 6 \pm 49\,\text{nb} \pm 29\%$ at $T_p = 1360\,\text{MeV}$ and $\sigma_{3\pi^0} = 115 \pm 3 \pm 23\,\text{nb} \pm 12\%$ at $T_p = 1450\,\text{MeV}$. The first error is statistical, the second is systematical and includes uncertainties from background and acceptance. The last uncertainty comes from the normalisation.

Background from quasi-free reactions $pp \rightarrow pp\,\pi^0\pi^0\pi^0$ with a proton misidentified as a ${}^3\text{He}$ is expected to be negligible. The probability that an event from a reaction with p or d in the final state instead of ${}^3\text{He}$ would survive the constraints, is smaller than 0.001%.

Invariant-mass distributions of the final-state particles in the $pd \rightarrow {}^3\text{He}\,\pi^0\pi^0\pi^0$ reaction give important information about the production mechanism. Deviation from phase space can give hints about, *e.g.*, intermediate resonances. In this work we have studied the $2\pi^0$-system, the ${}^3\text{He}\pi^0$-system and the ${}^3\text{He}2\pi^0$-system. When studying the invariant mass of two pions it is more convenient to instead reconstruct the missing mass of the ${}^3\text{He}$ and the third pion, here denoted $MM({}^3\text{He}\pi^0)$. This is because the ${}^3\text{He}$ is measured in the FD with higher resolution than the pions, which are measured in the CD.

In order to avoid an event sample with a lot of background from the $pd \rightarrow {}^3\text{He}\,\eta$ and $pd \rightarrow {}^3\text{He}\,\eta\pi^0$, events which fulfill the condition $600\,\text{MeV}/c^2 < MM({}^3\text{He}) < 700\,\text{MeV}/c^2$ are selected. $MM({}^3\text{He}\pi^0)$ is then reconstructed for these events. In this event sample, there will be a small contribution (a few percent) from the $pd \rightarrow {}^3\text{He}\,\eta\pi^0$, $\eta \rightarrow 3\pi^0$ reaction and the data will therefore be subtracted by the expected amount of $\eta\pi^0$, $\eta \rightarrow 3\pi^0$ events, obtained from simulations. The data are
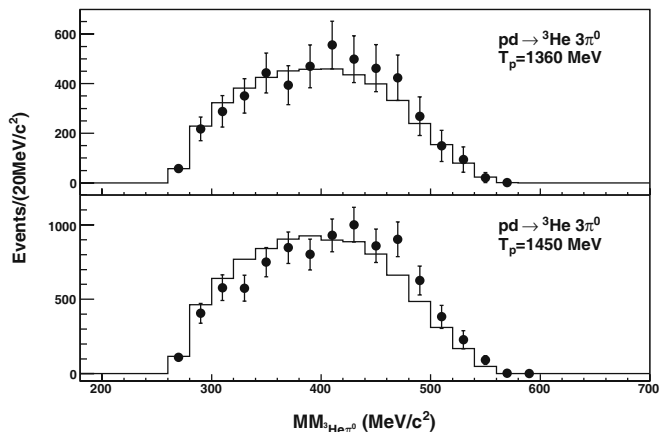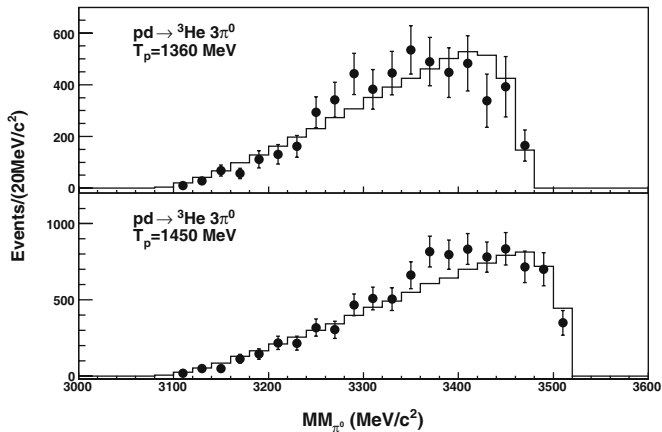

Fig. 8. The missing mass of the ${}^3\text{He}\pi^0$-system, which is equivalent to the invariant mass of the $2\pi^0$-system. The points represent background-subtracted and acceptance-corrected data satisfying the criteria given in the text and $600\,\text{MeV}/c^2 < MM({}^3\text{He}) < 700\,\text{MeV}/c^2$. The solid histogram shows phase space Monte Carlo simulations of $3\pi^0$ production. The upper panel shows the $T_p = 1360\,\text{MeV}$ case and the lower one the $T_p = 1450\,\text{MeV}$ case.
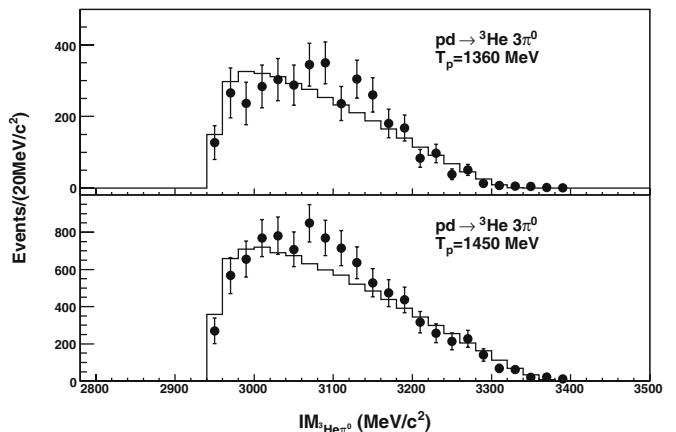
Fig. 9. The invariant mass of the ${}^3\text{He}\pi^0$-system. The points represent background-subtracted and acceptance-corrected data, fulfilling the constraints given in the text and $600\,\text{MeV}/c^2 < MM({}^3\text{He}) < 700\,\text{MeV}/c^2$. The solid histogram shows phase space Monte Carlo simulations of $3\pi^0$ production. The upper panel shows the $T_p = 1360\,\text{MeV}$ case and the lower one the $T_p = 1450\,\text{MeV}$ case.

then corrected for acceptance. The results are shown in the upper and lower panel of fig. 8. The points represent the background-subtracted and acceptance-corrected data and the solid histogram phase-space-simulated $3\pi^0$ data. The experimental data follow phase space well.

The invariant mass of the ${}^3\text{He}\pi^0$-system, $IM({}^3\text{He}\pi^0)$, has also been reconstructed. The small background from $\eta\pi^0$ was subtracted in the same way as in the $MM({}^3\text{He}\pi^0)$ case and the data was then corrected for acceptance. The result is shown in fig. 9. Here the data disagree with phase space. There is an enhancement with respect to phase space centered around $\approx 3090\,\text{MeV}/c^2$, which roughly

Fig. 10. The missing mass of the π^0, which is equivalent to the invariant mass of the $^3\text{He}2\pi^0$-system. The points represent background-subtracted and acceptance-corrected data fulfilling the constraints given in the text and $600\,\text{MeV}/c^2 < MM(^3\text{He}) < 700\,\text{MeV}/c^2$. The solid histogram shows phase space Monte Carlo simulations of $3\pi^0$ production. The upper panel shows the $T_p = 1360\,\text{MeV}$ case and the lower one the $T_p = 1450\,\text{MeV}$ case.

equals the sum $2m_p + M_{\Delta(1232)}$. This may indicate a single $\Delta(1232)$ excitation in the production process.

Finally, the invariant mass of the $^3\text{He}\pi^0\pi^0$-system is studied. This is done by reconstructing the missing mass of one of the π^0 mesons. In this way, the resolution is improved. The experimental data were background subtracted, using simulated $pd \rightarrow {}^3\text{He}\eta\pi^0$, $\eta \rightarrow 3\pi^0$ data, and acceptance corrected. The result is shown in fig. 10, together with the phase space Monte Carlo simulations of $pd \rightarrow {}^3\text{He}\pi^0\pi^0\pi^0$. There is a small enhancement at high $MM(\pi^0)$ around the $2m_p + M_{N^*(1440)}$ sum, which may indicate the involvement of a Roper $N^*(1440)$ excitation in the production mechanism.

4.2 $pd \rightarrow {}^3\text{He}\,\pi^+\pi^-\pi^0$

All selection criteria optimised for $\eta \rightarrow \pi^+\pi^-\pi^0$ selection, given in table 3 in sect. 3.1.3, are applied. In addition, we require that both charged pions are emitted in directions covered by the CD, *i.e.* that no other charged tracks than the ^3He are found in the FD. Finally, two charged tracks in the MDC are required, with overlapping hits in the PSB. The total acceptance, calculated partly using Monte Carlo simulations (all constraints not involving the MDC, see sect. 3.1.3) and partly analysing $\omega \rightarrow \pi^+\pi^-\pi^0$ data (all constraints involving the MDC, see ref. [23]) is 7.2% at 1360 MeV and 6.7% at 1450 MeV.

In fig. 11, the missing mass of the ^3He is shown for all events satisfying the criteria given in table 4. There is a small enhancement around the η mass and a clear peak at the ω mass, but except from that, the experimental data seem to follow the phase space $\pi^+\pi^-\pi^0$ distribution well. There is no sign of any $pd \rightarrow {}^3\text{He}\,\eta\pi^0$, $\eta \rightarrow \pi^+\pi^-\pi^0$ events in this sample. The acceptance for this reaction
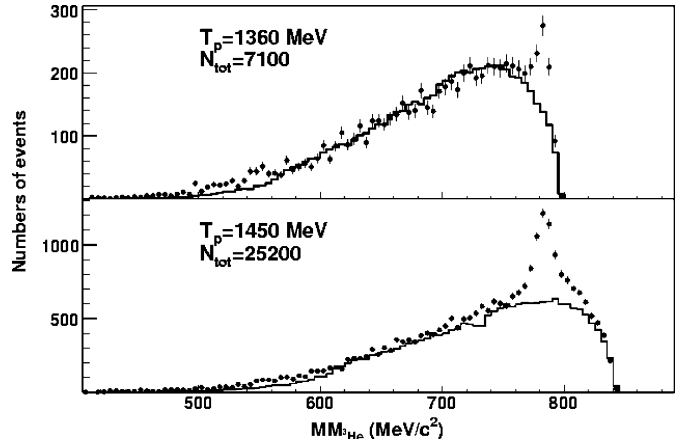

Fig. 11. The upper panel shows the WASA data sample fulfilling the constraints optimised for the selection of $pd \rightarrow {}^3\text{He}\,\pi^+\pi^-\pi^0$ at 1360 MeV and the lower panel shows the 1450 MeV case. The solid line histograms show Monte-Carlo–simulated $pd \rightarrow {}^3\text{He}\,\pi^+\pi^-\pi^0$ data fulfilling the given constraints. The peak in the experimental data at high missing masses are $pd \rightarrow {}^3\text{He}\,\omega$, $\omega \rightarrow \pi^+\pi^-\pi^0$ events. The spectra are not corrected for acceptance and the background simulations are scaled to fit the data.

Table 4. The constraints applied for the selection of $pd \rightarrow {}^3\text{He}\,\pi^+\pi^-\pi^0$.

^3He giving signal in the FPC and stopping in the FRH
$\geqslant 2$ photons in the SEC;
one $\gamma\gamma$-combination fulfilling $|IM(\gamma\gamma) - m_{\pi^0}| < 45\,\text{MeV}/c^2$;
$MM(^3\text{He}\pi^0) > 250\,\text{MeV}/c^2$;
$\geqslant 2$ hits in the PSB;
$E_{tot}(\text{SEC}) < 900\,\text{MeV}$;
no $\pi^\pm$ in FD;
2 MDC tracks with matching hits in the PSB

when applying the cuts in table 4 is 9% at 1360 MeV and 12% at 1450 MeV. At the higher energy, where the $\eta\pi^0$ cross-section is known (see [26]), the expected number of $pd \rightarrow {}^3\text{He}\,\eta\pi^0$, $\eta \rightarrow \pi^+\pi^-\pi^0$ events is ≈ 250, which constitute only $\approx 1\%$ of the continuum data in the lower panel of fig. 11. In the previous section we found that the direct $4\pi^0$ cross-section at 1450 MeV must be very small, and even if the cross-section of direct $\pi^+\pi^-\pi^0\pi^0$ is likely higher than the direct $4\pi^0$ cross-section due to more possible isospin amplitudes, it is reasonable to assume that direct $\pi^+\pi^-\pi^0\pi^0$ production will give a negligible contribution to our $\pi^+\pi^-\pi^0$ data sample. This assumption is also very well in line with the good agreement between data and simulations in fig. 11. The number of $\pi^+\pi^-\pi^0$ events at 1360 MeV, $N_{3\pi} = 6700$, corresponds to a total cross-section of 1400 nb. This is obtained using an acceptance which is calculated assuming phase space production, but since the WASA detector covers the major part of the ^3He phase space for this reaction, the model dependence of the acceptance is small.
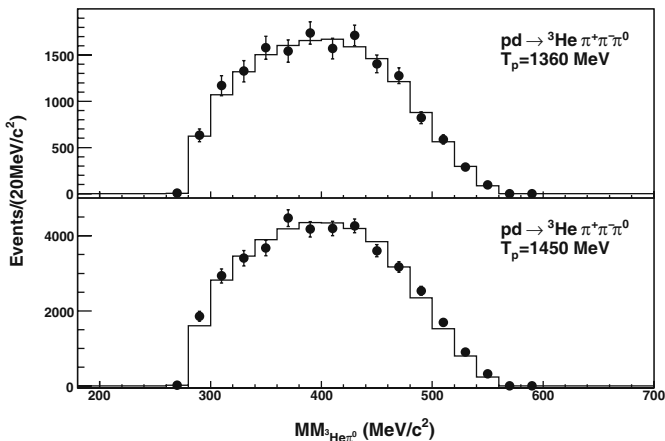
Fig. 12. The missing mass of the ${}^3\text{He}\pi^0$-system. The points represent acceptance-corrected data satisfying the criteria given in the text and $600\,\text{MeV}/c^2 < MM({}^3\text{He}) < 700\,\text{MeV}/c^2$. The solid histogram shows phase space Monte Carlo simulations of $\pi^+\pi^-\pi^0$ production. The upper panel shows the $T_p = 1360\,\text{MeV}$ case and the lower one the $T_p = 1450\,\text{MeV}$ case.

Fig. 13. The invariant mass of the ${}^3\text{He}\pi^0$-system. The points represent acceptance-corrected data fulfilling the constraints given in the text and $600\,\text{MeV}/c^2 < MM({}^3\text{He}) < 700\,\text{MeV}/c^2$. The solid histogram shows phase space Monte Carlo simulations of $\pi^+\pi^-\pi^0$ production. The upper panel shows the $T_p = 1360\,\text{MeV}$ case and the lower one the $T_p = 1450\,\text{MeV}$ case.

The largest contribution to the systematic uncertainty comes from the efficiency of the MDC. A robust method of estimating this uncertainty is to calculate the cross-section with and without using the information from the MDC, treat the difference as a systematical uncertainty and assume that it is symmetric.

At 1360 MeV, the number of $\pi^+\pi^-\pi^0$ events obtained using selection criteria without involving the MDC is $N_{3\pi} = 33000$ and the acceptance is 28%. This corresponds to a cross-section of 1770 nb which gives a systematical uncertainty of 370 nb.

There may be a systematic uncertainty arising from falsely identified $pd \to {}^3\text{He}\eta\pi^0$, $\eta \to \pi^+\pi^-\pi^0$. According to the rough upper limit of the $\eta\pi^0$ cross-section at 1360 MeV that was given in the previous section, the maximum number of $\eta\pi^0$ events in this sample is 56. This gives a systematic uncertainty of 12 nb and is thus very small compared to the uncertainty from the MDC efficiency.

The statistical uncertainty is obtained by the square root of the total number of events and is determined to 17 nb. Finally, we get $\sigma_{\pi^+\pi^-\pi^0} = 1400 \pm 17 \pm 370\,\text{nb} \pm 29\%$ at $T_p = 1360\,\text{MeV}$.

Following the same reasoning at 1450 MeV, except that the $\eta\pi^0$ cross-section is known with good precision, the cross-section becomes $\sigma_{\pi^+\pi^-\pi^0} = 910 \pm 7 \pm 80\,\text{nb} \pm 12\%$.

As in the $3\pi^0$ case, the distributions of the final-state particles have been studied. Since the π^0 is the only pion that is fully reconstructed, the invariant mass of the $\pi^+\pi^-$-system is studied by reconstructing the missing mass of the ${}^3\text{He}\pi^0$-system. To have a sample as similar to the $3\pi^0$ case as possible, events which satisfy $600\,\text{MeV}/c^2 < MM({}^3\text{He}) < 700\,\text{MeV}/c^2$ are selected. The $MM({}^3\text{He}\pi^0)$ is reconstructed and the data are corrected for acceptance. Note that no background subtraction had to be made in this case, since the contribution from $pd \to {}^3\text{He}\eta\pi^0$ is proven to be small at both energies. The results at both energies are shown in fig. 12.
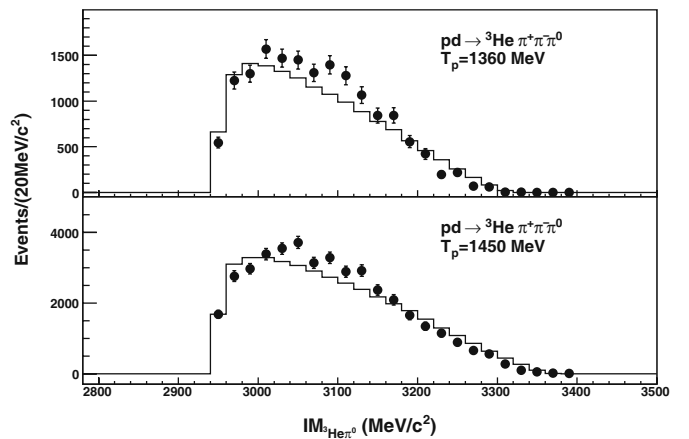
There is good agreement between experiment and simulated $\pi^+\pi^-\pi^0$ data and there is no sign of any intermediate ρ meson, which would push the $MM({}^3\text{He}\pi^0)$ towards higher masses. This is not surprising since despite the large width of the ρ meson ($\Gamma \approx 150\,\text{MeV}$), we are far below the nominal $pd \to {}^3\text{He}\rho^0\pi^0$ threshold at both beam energies considered in this work.

The invariant mass of the ${}^3\text{He}\pi^0$ is reconstructed in the same way as in the $3\pi^0$ case, except that no background subtraction was necessary. The results are shown in fig. 13. Also in the $\pi^+\pi^-\pi^0$ case, there is a small enhancement around the $2m_p + M_{\Delta(1232)}$ sum.

The invariant mass of the ${}^3\text{He}\pi^+\pi^-$-system is studied by reconstructing the missing mass of the π^0. The acceptance-corrected data are shown in fig. 14. Like in the $pd \to {}^3\text{He}\pi^0\pi^0\pi^0$ case, there is a small enhancement with respect to phase space near the $2m_p + M_{N^*(1440)}$ sum, suggesting that the Roper resonance $N^*(1440)$ may be involved in the production process.

4.3 Comparison between the pd → ^{3}He $\pi^+\pi^-\pi^0$ and the pd → ^{3}He $\pi^0\pi^0\pi^0$ reactions

In the introduction, the ratio between the cross-sections of the $pd \to {}^3\text{He}\,\pi^+\pi^-\pi^0$ and the $pd \to {}^3\text{He}\,\pi^0\pi^0\pi^0$ reactions, *i.e.* $\frac{\sigma(pd \to {}^3\text{He}\,\pi^+\pi^-\pi^0)}{\sigma(pd \to {}^3\text{He}\,\pi^0\pi^0\pi^0)}$, was calculated to 9, using a statistical model where all isospin amplitudes $M_{T_{3\pi}}$ are put equal and all cross terms are set to zero. If instead $M_0 = 0$, the ratio becomes 4. In this work, the ratio has been measured experimentally at both energies. By using the cross-sections determined in sects. 4.1 and 4.2, one then obtains 7.8 at 1360 MeV and 7.9 at 1450 MeV for this ratio. However, to give a comparison at the same excess energy Q, the results have to be corrected for the difference between the masses of the $\pi^\pm$ and π^0. The
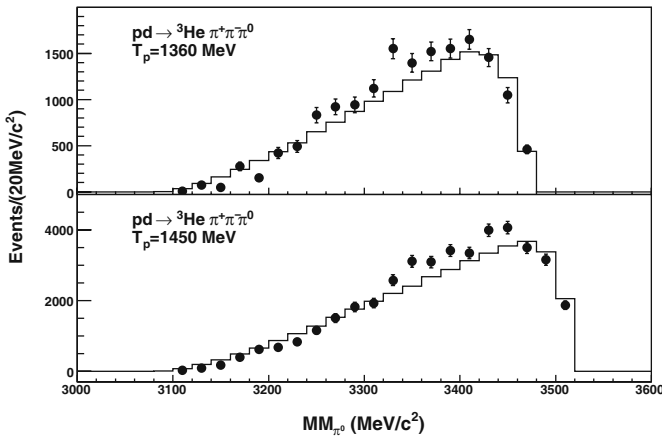
Fig. 14. The missing mass of the π^0. The points represent acceptance-corrected data fulfilling the constraints given in the text and $600\,\mathrm{MeV}/c^2 < MM(^3\mathrm{He}) < 700\,\mathrm{MeV}/c^2$. The solid histogram shows phase space Monte Carlo simulations of $\pi^+\pi^-\pi^0$ production. The upper panel shows the $T_p = 1360\,\mathrm{MeV}$ case and the lower one the $T_p = 1450\,\mathrm{MeV}$ case.

lower mass of the π^0 makes the phase space volume of the $pd \to {}^3\mathrm{He}\,\pi^0\pi^0\pi^0$ reaction larger than that of the $pd \to {}^3\mathrm{He}\,\pi^+\pi^-\pi^0$ at the same beam energy. After correcting for the difference in phase space volume, the ratio becomes $8.3 \pm 0.3 \pm 3.1$ at $1360\,\mathrm{MeV}$ and $8.4 \pm 0.2 \pm 1.8$ at $1450\,\mathrm{MeV}$, where the first uncertainty is statistic and the second systematic. Note that the uncertainty in the normalisation cancels in the ratio. The values obtained are consistent with the value of 9 predicted using the statistical approach. The interpretation of this result is then that M_0 should be of similar size as M_1.

5 Summary and conclusions

The production of light mesons, *i.e.* π and η, have been studied at $T_p = 1360\,\mathrm{MeV}$ and $T_p = 1450\,\mathrm{MeV}$. The $pd \to {}^3\mathrm{He}\,\eta$ reaction was studied by using data from the three most common decay channels; $\eta \to \gamma\gamma$, $\eta \to \pi^0\pi^0\pi^0$ and $\eta \to \pi^+\pi^-\pi^0$. The result from the different channels gave consistent results. At both energies, the angular distributions of the η meson were reconstructed and they show a pronounced forward-backward asymmetry. The WASA detector does not cover the full angular range at these high energies and one could therefore not say whether the forward plateau or dip observed in [7,8] persists at high energies. The data from this work in combination with data taken at the same energy with the SPES III spectrometer [12] do, however, suggest that the forward dip persists at this high energy and is stronger compared to the lower energy case. If not, the $1450\,\mathrm{MeV}$ data from this work disagree with the SPES III data in the forward hemisphere.

The total cross-sections of three-pion production in $pd \to {}^3\mathrm{He}\,\pi^0\pi^0\pi^0$ and $pd \to {}^3\mathrm{He}\,\pi^+\pi^-\pi^0$ were measured at both energies. The ratio between the $\pi^+\pi^-\pi^0$

Table 5. The total cross-sections of the reactions studied in this work. In addition to the systematic uncertainty given in the table, there is a normalisation uncertainty of 29% at $1360\,\mathrm{MeV}$ and 12% at $1450\,\mathrm{MeV}$. The normalisation is made using $pd \to {}^3\mathrm{He}\,\eta$ data and differential cross-sections given in [11,12].

Reaction	T_p	σ	stat.	syst.
	(MeV)	(nb)	(nb)	(nb)
$pd \to {}^3\mathrm{He}\,\eta$	1360	151.6	± 9.3	± 35.2
$pd \to {}^3\mathrm{He}\,\pi^0\pi^0\pi^0$	1360	180	± 6	± 49
$pd \to {}^3\mathrm{He}\,\pi^+\pi^-\pi^0$	1360	1400	± 17	± 370
$pd \to {}^3\mathrm{He}\,\eta$	1450	80.8	± 3.6	± 43.1
$pd \to {}^3\mathrm{He}\,\pi^0\pi^0\pi^0$	1450	115	± 3	± 23
$pd \to {}^3\mathrm{He}\,\pi^+\pi^-\pi^0$	1450	910	± 7	± 80

and $3\pi^0$ cross-sections was calculated at both energies and the results are consistent with the statistical model, where $M_0 = M_1$ and all cross terms are neglected. The invariant-mass distributions of the two-pion system and the ${}^3\mathrm{He}\pi^0$-system were reconstructed. The invariant-mass distributions of the two-pion system follow phase space but the corresponding distribution of the ${}^3\mathrm{He}\pi^0$-system, show a small enhancement around the $2m_p + M_{\Delta(1232)}$ mass. This enhancement was observed in $3\pi^0$ and $\pi^+\pi^-\pi^0$ production at both energies and may indicate a single Δ excitation in the production mechanism.

The invariant-mass distributions of the ${}^3\mathrm{He}2\pi$-system, for both $\pi^+\pi^-\pi^0$ and $3\pi^0$ production at both energies, show an enhancement near the $2m_p + M_{N^*(1440)}$ mass, suggesting that the Roper $N^*(1440)$ resonance may be involved in the production mechanism.

The cross-sections measured in this work are summarised in table 5.

References

1. J. Berger *et al.*, Phys. Rev. Lett. **61**, 919 (1988).
2. B. Mayer *et al.*, Phys. Rev. C **53**, 2068 (1996).
3. T. Mersmann *et al.*, Phys. Rev. Lett. **98**, 242301 (2007).
4. J. Smyrski *et al.*, Phys. Lett. B **649**, 258 (2007).
5. H.-H Adam *et al.*, Phys. Rev. C **75**, 014004 (2007).
6. C. Wilkin, Phys. Rev. C **47**, R938 (1993).

7. R. Bilger *et al.*, Phys. Rev. C **65**, 044608 (2002).
8. T. Rausmann *et al.*, Phys. Rev. C **80**, 017001 (2009).
9. M. Betigeri *et al.*, Phys. Lett. B **472**, 267 (2000).
10. J. Banaigs *et al.*, Phys. Lett. B **45**, 394 (1973).
11. P. Berthet *et al.*, Nucl. Phys. A **443**, 589 (1985).
12. T. Kirchner, PhD Thesis, IPN Orsay, France (1993).
13. R.M. Sternheimer, S.J. Lindenbaum, Phys. Rev. **123**, 333 (1961).
14. G. Alexander *et al.*, Phys. Rev. **154**, 1284 (1967).
15. A.P. Colleraine, U. Nauenberg, Phys. Rev. **161**, 1387 (1967).
16. S.P. Almeida *et al.*, Phys. Rev. **174**, 1638 (1968).
17. C. Pauly *et al.*, Phys. Lett. B **649**, 122 (2007).
18. E. Fermi, Prog. Theor. Phys. **5**, 570 (1950).
19. Chr. Bargholtz *et al.*, Nucl. Instrum. Methods A **594**, 339 (2008).
20. C. Ekström *et al.*, Physica Scr. T **99**, 169 (2002).
21. Ö. Nordhage PhD Thesis, Uppsala University, Sweden (2006).
22. H. Calén *et al.*, Nucl. Instrum. Methods A **379**, 57 (1996).
23. K. Schönning, PhD Thesis, Uppsala University, Sweden (2009).
24. K. Schönning *et al.*, Acta Phys. Slovaca **56**, No. 3, 299 (2006).
25. K. Schönning *et al.*, Phys. Rev. C **79**, 044002 (2009).
26. K. Schönning *et al.*, Phys. Lett. B **685**, 33 (2010).